DOI 10.1007/s10778-020-01036-4
International Applied Mechanics, Vol. 56, No. 5, September, 2020

EFFECT OF THE THIRD APPROXIMATION IN THE ANALYSIS OF THE EVOLUTION OF A NONLINEAR ELASTIC P-WAVE. PART 1*

J. J. Rushchitsky* and V. N. Yurchuk

A nonlinear plane longitudinal elastic displacement wave is studied theoretically and numerically using the Murnaghan model for two forms of initial profile: harmonic and bell-shaped. A major novelty is that the evolution of waves is analyzed by approximate methods taking into account the first three approximations. The harmonic wave is analyzed only to compare with the new results for the bell-shaped wave. Some significant differences between the evolution of waves are shown. The initially symmetric profiles transform differently due to distortion: symmetrically (for the harmonic profile) and asymmetrically (for the bell-shaped profile). The third approximation introduces the fourth harmonic for the harmonic wave when this wave is analyzed by the method of successive approximations, while the bell-shaped wave is characterized in the third approximation differently when using the method of constraints on the displacement gradient. At relatively long distances from the beginning of the propagation, the one-hump bell-shaped wave transforms into a two-hump one. These humps adjoin each other halving their lengths. The third approximation allows us to observe new wave effects: the asymmetry of the left and right humps about their peaks and the asymmetry of the humps about each other; the lowering of the left hump and the rise of the right one. The results obtained are analyzed.

Keywords: nonlinear elastic P-wave; Murnaghan potential; approximate method; harmonic and bell-shaped initial wave profiles; evolution; distortion

1. Introduction. In the presented study, the five-constant Murnaghan model of nonlinear elastic deformation of a material is used [1–3, 5, 7–11]. The Murnaghan elastic potential is known to be quadratically and cubically nonlinear in the components of the Cauchy–Green strain tensor $\varepsilon_{nm} = (1/2)(u_{n,m} + u_{m,n} + u_{k,n}u_{k,m})$ (u_k are the components of the displacement vector)

$$W(\varepsilon_{ik}) = (1/2)\lambda(\varepsilon_{mm})^2 + \mu(\varepsilon_{ik})^2 + (1/3)A\varepsilon_{ik}\varepsilon_{im}\varepsilon_{km} + B(\varepsilon_{ik})^2\varepsilon_{mm} + (1/3)C(\varepsilon_{mm})^3 \tag{1}$$

(λ, μ, A, B, C are the Murnaghan elastic constants).

We consider the case where the Murnaghan potential is expressed in terms of the displacement gradients taking into account only the quadratically and cubically nonlinear components:

$$W = (1/2)\lambda(u_{m,m})^2 + (1/4)\mu(u_{i,k} + u_{k,i})^2 + \left(\mu + (1/4)A\right)u_{i,k}u_{m,i}u_{m,k}$$

S. P. Timoshenko Institute of Mechanics, National Academy of Sciences of Ukraine, 3 Nesterova St., Kyiv, Ukraine 03057; *e-mail: rushch@inmech.kiev.ua. Translated from Prikladnaya Mekhanika, Vol. 56, No. 5, pp. 65–77, September–October 2020. Original article submitted October 30, 2019.

* This study was sponsored by the budget program "Support for Priority Areas of Scientific Research" (KPKVK 6541230).

$$+(1/2)(\lambda+B)u_{m,m}(u_{i,k})^2+(1/12)Au_{i,k}u_{k,m}u_{m,i}+(1/2)Bu_{i,k}u_{k,i}u_{m,m}+(1/3)C(u_{m,m})^3. \quad (2)$$

We consider motion in which the displacements depend only on one spatial coordinate and time $u_k = u_k(x_1, t)$ (displacements along the Ox_1 axis in the Cartesian coordinate system $Ox_1x_2x_3$). In this case, potential (2) is simplified:

$$W = (1/2)\left[(\lambda+2\mu)(u_{1,1})^2+\mu\left[(u_{2,1})^2+(u_{3,1})^2\right]\right]$$

$$+\left[\mu+(1/2)\lambda+(1/3)A+B+(1/3)C\right](u_{1,1})^3+(1/2)(\lambda+B)u_{1,1}\left[(u_{2,1})^2+(u_{3,1})^2\right]. \quad (3)$$

From (3) nonlinear wave equations are obtained for three types of polarized plane waves (P-, SH-, SV- waves). The simplest nonlinear wave equations are quadratically nonlinear. In particular, the motion of a P-wave is described by the equation

$$\rho u_{1,tt}-(\lambda+2\mu)u_{1,11}=N_1u_{1,11}u_{1,1}+N_2(u_{2,11}u_{2,1}+u_{3,11}u_{3,1}), \quad (4)$$

$$N_1=\left[3(\lambda+2\mu)+2(A+3B+C)\right], \qquad N_2=\lambda+2\mu+(1/2)A+B. \quad (5)$$

Further, the analysis is limited to the problem where only a P-wave is initially excited in a material [2] and the main nonlinear phenomenon is self-generation of waves. Then the nonlinear equation (4) takes the form

$$\rho u_{1,tt}-(\lambda+2\mu)u_{1,11}=N_1u_{1,11}u_{1,1}\rightarrow u_{1,tt}-(v_L)^2u_{1,11}=(N_1/\rho)u_{1,11}u_{1,1}, \quad (6)$$

where $v_L=\sqrt{(\lambda+2\mu)/\rho}$ is the phase velocity of the P-wave in the linear approximation.

Up to now, Eqs. (6) have been analyzed approximately using three methods of successive approximations, slowly varying amplitudes, constraints on the displacement gradient [1–3, 5, 7–15]. Harmonic waves and solitary waves with different initial profiles were studied. Most of the results are related to the analysis of the nonlinear behavior of waves in the first two approximations. Harmonic waves, however, were studied in many approximations [8, 9, 12]. However, the features of wave evolution are most clearly revealed in numerical simulation only. Since such a problem includes many parameters and the results are strongly dependent on the choice of material, wavelength, and wave amplitude, the resulting scenarios of wave evolution differ quite significantly. Therefore, any new numerical results obtained for new materials or new wave parameters always complement the general picture of evolution.

In this study, the harmonic and bell-shaped profiles are selected to study the evolution of the bell-shaped wave. The harmonic wave plays an auxiliary role here, although it has been analyzed numerically for new materials. The purpose of combining the analysis for the two profiles is to compare the scenarios of harmonic and solitary waves with symmetrical profiles. The main innovation in the analysis of a solitary wave is the inclusion of the third approximation. It should be noted that the use of the third approximation has already been analyzed earlier for other materials, where it was found that the decisive factor for revealing a observable evolution effect is the distance traveled by the wave.

2. Approximate Approach to the Analysis of the Evolution of the Initial Wave Profile Using the Nonlinear Wave Equation (6). The problem of the evolution of a harmonic wave was studied earlier by the method of successive approximations [1–3, 8]. According to the method, the recurrence relation $u_{1,tt}^{(n)}-(v_L)^2u_{1,11}^{(n)}=(N_1/\rho)u_{1,11}^{(n-1)}u_{1,1}^{(n-1)}$ is used to determine any approximation, and the solution is represented as

$$u_1(x_1,t)=\sum_{n=1}^{\infty}u_1^{(n)}(x_1,t)=u_1^{(1)}(x_1,t)+u_1^{(2)}(x_1,t)+u_1^{(3)}(x_1,t)+\ldots.$$

The solution for zero approximation is linear and has the following form for given initial maximum amplitude $u_{1(0)}$, wave number k_L, and frequency ω [1–3, 11]:

$$u_1^{(1)}(x,t)=u_{1(1)}\cos(k_Lx-\omega t)\left((\omega/k_L)=v_L\right). \quad (7)$$

The corresponding solution for the first approximation is as follows [1–3, 8, 11]:

$$u_1^{(2)}(x_1,t)=\left[N_1/8(\lambda+2\mu)\right](u_{1(0)})^2 k_L^2 x_1\cos 2(k_L x_1-\omega t). \tag{8}$$

Thus, the second-order solution has the form

$$u_1^{(1+2)}(x,t)=u_{1o}\cos\sigma+u_{1o}M_L x_1\cos 2\sigma,$$

$$M=\frac{N_1}{8(\lambda+2\mu)}u_{1o}(k_L)^2=\frac{1}{8\rho}N_1u_{1o}\frac{k_L^2}{v_L^2}=\frac{1}{8\rho}N_1u_{1o}\frac{\omega^2}{v_L^4}.$$

The third approximation is as follows [9, 10]:

$$u_1^{(3)}=u_{1(0)}(M_L)^3(x_1)^3\left\{-\frac{8}{3}+\frac{13}{2k_Lx_1}\sin 4\sigma+\left[-\frac{4}{3}+\frac{29}{8(k_L)^2(x_1)^2}\right]\cos 4\sigma\right\}. \tag{9}$$

Thus, the third approximation introduces the fourth harmonic into the solution. Accordingly, the fourth approximation will introduce the eighth harmonic (at each step, the harmonics are doubled).

The solution within the first three approximations has the following form [8–11]:

$$u_2^{(1+2+3)}(x_1,t)=u_1^{(0)}(x_1,t)+u_1^{(1)}(x_1,t)+u_1^{(2)}(x_1,t)=u_{1o}\cos\sigma+u_{1o}M_Lx_1\cos 2\sigma$$

$$+u_{1o}(M_L)^3(x_1)^3\left[-\frac{8}{3}+\frac{5}{2k_Lx_1}\sin 4\sigma+\left(-\frac{4}{3}+\frac{11}{8(k_Lx_1)^2}\right)\cos 4\sigma\right]. \tag{10}$$

Thus, the evolution in three approximations is determined by the parameter M_L, the initial amplitude, and the wave number in the linear approximation. Next, we will perform a numerical simulation of the evolution of a harmonic wave for two new materials and compare with a similar study of a bell-shaped wave.

According to [8–11], the analysis of the evolution of solitary waves by the method of successive approximations involves severe mathematical difficulties; therefore, the method of constraint on the displacement gradient will be applied to the analysis of the bell-shaped wave. To this end, we write Eq. (7) as

$$u_{1,tt}-\{(v_L)^2+(N_1/\rho)u_{1,1}\}u_{1,11}=0\rightarrow u_{1,tt}-\{1+\alpha u_{1,1}\}(v_L)^2u_{1,11}=0,$$

$$\alpha=\left[N_1/(\lambda+2\mu)\right]. \tag{11}$$

According to the method, the initial wave profile is described by a sufficiently smooth function $u(x_1,t=0)=F(x_1)$ and the wave propagates as a D'Alembert wave:

$$u(x_1,t)=F(x_1-vt), \tag{12}$$

where the variable velocity of the wave is defined by

$$v=\sqrt{1+\alpha u_{1,1}}\,c_L. \tag{13}$$

At the next step, the root in (13) is written as a series

$$\sqrt{1+\alpha u_{1,1}}=(1+\alpha u_{1,1})^{1/2}=1+(1/2)\alpha u_{1,1}-(1/8)(\alpha u_{1,1})^2+\ldots,$$

where

$$|\alpha u_{1,1}|<1. \tag{14}$$

The smallness of $\alpha u_{1,1}$ allows us to represent the approximate solution (12) in the form of the first three approximations:

$$u_1(x_1,t) \cong F\{a(x_1 - v_L t) - (1/2)t\alpha v_L u_{1,1}[1-(1/4)\alpha v_L u_{1,1}]\}. \quad (15)$$

It should be noted that earlier the approximate solution had the form of the first two approximations. Therefore, approximation (15) introduces an element of novelty into the subsequent analysis.

The accuracy of (15) depends on how accurately condition (14) is satisfied, which includes constraints for two parameters: $\alpha = 3 + 2(A + 3B + C)/(\lambda + 2\mu)$ and $u_{1,1}$.

Denote the phase of a wave with constant phase velocity by $\sigma = a(x_1 - c_L t)$ and introduce the additional small parameter

$$|\delta| = \left| -(1/2)t\alpha v_L u_{1,1}\left[1-(1/4)\alpha v_L u_{1,1}\right]\right| << 1. \quad (16)$$

Solution (15) can be expanded into a Taylor series:

$$u(x_1,t) \approx F(\sigma+\delta) \approx F(\sigma) + F'(\sigma)\delta + (1/2)F''(\sigma)\delta^2 + \ldots. \quad (17)$$

We will further restrict the analysis to the first three terms in (17) due to the smallness of δ. Since the smallness of $|\alpha u_{1,1}|$ has already been assumed in (14), this is a constraint on $av_L t$.

Next, we need an expression for the displacement gradient, which can be easily derived from (17):

$$u_{1,1}(x_1,t) \approx F'_\sigma\ (\sigma+\delta)\cdot\sigma'_{x_1} = F'_\sigma\ (\sigma+\delta)\cdot\{a - (1/2)t\alpha v_L u_{1,11}[1-(1/2)t\alpha v_L]\} \approx aF'_\sigma\ (\sigma).$$

This expression allows us to write solution (16) in the form

$$u_1(x_1,t) \approx F(\sigma) - F'_{,1}\ (\sigma)a^2\{(1/2)t\alpha v_L F'_{,1}\ (\sigma)[1-(1/4)\alpha a F'_{,1}\ (\sigma)]\}$$

$$= F(\sigma) - (1/2)\alpha a^2 v_L t[F'_{,1}(\sigma)]^2\left[1-(1/4)\alpha a v_L F'_{,1}\ (\sigma)\right]. \quad (18)$$

The approximate solution (18) is general, and for different specific functions F, it describes nonlinear wave effects such as occurrence of the second and third harmonics of a harmonic wave or new similar components of a solitary wave and increasing amplitude with time.

Next, the wave profile is considered to have the form of a Gaussian function $F(x_1) = e^{-((ax_1)^2/2)}$ (bell-shaped solitary wave). For a solitary wave, a is the wavelength. This parameter is important for assessing the correlation of the wave to the model of small or large displacement gradients. The ratio of the maximum wave amplitude to the length just allows us to make such an estimate.

3. Parameters of the Material and Wave in Numerical Simulation. Let us choose two metal composite materials (matrix–aluminum, filler–tungsten) with the following mechanical parameters (SI system) [1, 8]:

Material 51 (the volume fraction of the matrix is 0.8)

$$\rho = 0.594\cdot 10^{-4}, \quad \lambda = 5.59\cdot 10^{-10}, \quad \mu = 3.26\cdot 10^{-10},$$

$$A = -0.658\cdot 10^{-11}, \quad B = -2.18\cdot 10^{-11}, \quad C = -4.35\cdot 10^{-11},$$

$$c_L = 4.515\cdot 10^3, \quad \alpha = -16.072.$$

Material 52 (the volume fraction of the matrix is 0.6)

$$\rho = 0.918\cdot 10^{-4}, \quad \lambda = 11.6\cdot 10^{-10}, \quad \mu = 0.721\cdot 10^{-10},$$

$$A = -1.33\cdot 10^{-11}, \quad B = -4.45\cdot 10^{-11}, \quad C = -9.5\cdot 10^{-11},$$

$$c_L = 3.769\cdot 10^3, \quad \alpha = -34.08.$$

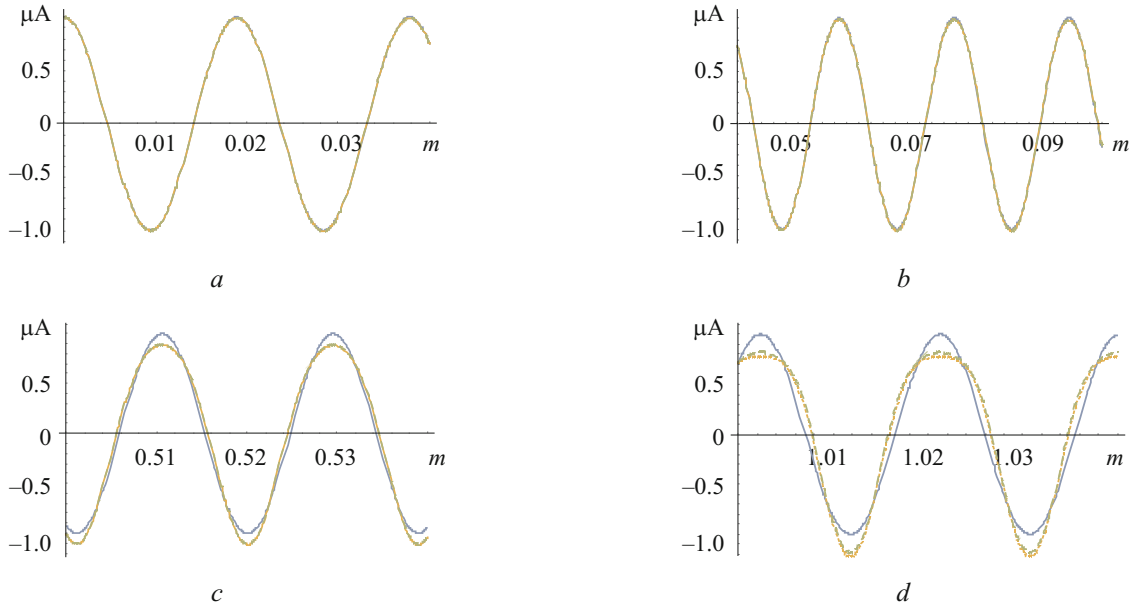

Fig. 1

The parameters of the harmonic wave are as follows: the wave velocity $c_L = (\omega / k_L)$ chosen earlier; the initial frequency ω selected from the ultrasonic wavelength range was used to calculate the wave number $k_L = (\omega / c_L)$ and the wavelength by the formula $L = (2\pi / k_L)$ (individual wavelength for each material) $\omega = 1.5 \cdot 10^6$, $L = 0.018$ (material 51); $\omega = 1.5 \cdot 10^6$, $L = 0.015$ (material 52).

For a solitary wave with a profile described by a Gaussian function (which is a weight function), it is assumed that the wavelength L is the interval (distance) for which the area outside this interval under the graph of the initial wave profile is negligible.

Then, according to the 3σ-rule, the length of the Gaussian (bell-shaped) wave $e^{-(x^2/2\sigma^2)} = e^{-[(x/\sigma)^2/2]}$ is equal to 6σ. Therefore, in the profile $F(x_1) = e^{-[(a\,x_1)^2/2]}$, the parameter a determines the wavelength by the formula $\sigma = (1/a)$. For the two materials chosen, the initial wavelength is the same: $L = \{0.0375, 0.0187\}$.

Consider 16 cases of the initial parameters of a P-wave (2 materials, 2 analytical representations of the profile, 2 wavelengths, 2 initial amplitudes).

4. Numerical Analysis of a Harmonic Wave. Formula (10) was used to plot two-dimensional curves of displacement u_1 versus traveled distance x_1. Eight sets of plots (two materials, two wavelengths, two maximum initial amplitudes) were considered. Each set includes graphs with profiles that are superimposed on one another to compare approximations. The graphs differ in the wave profile for different distances: from the initial position of the wave to the position at a distance of approximately 20 wavelengths where the effect of nonlinearity and the distortion of the wave profile are significant.

Figure 1 shows the curves for M51 material, $L = 0.018$, $\omega = 1.5 \cdot 10^6$, $a_o = 1 \cdot 10^{-6}$.

Figure 1*a* corresponds to the initial stage of wave motion for all three approximations. Figure 1*b* corresponds to the stage of wave motion when nonlinearity is just beginning to manifest. Figure 1*c* corresponds to longer wave motion (approximately at a distance of 15 wavelengths) and the first approximation (the upper line for positive amplitude values), first + second approximations (the lower line for positive amplitude values), and the first + second + third approximations (the line for positive amplitude values, which coincides with the second one on the given interval). Figure 1*d* corresponds to twice as long wave motion (about 30 wavelengths) and the first approximation (the upper line for positive amplitude values), first + second approximations (the middle line for positive amplitude values), and first + second + third approximations (the lower line for positive amplitude values).

It follows from the graphs that the evolution of the initial wave profile occurs symmetrically about the tops of the curves. Figure 1*b* shows that when the wave moves over distances of five wavelengths, the nonlinearity of the material can be ignored. However, Fig. 1 shows only the initial stage of evolution and the main trend of evolution is not yet visible. In the next case, such a trend is already quite obvious.

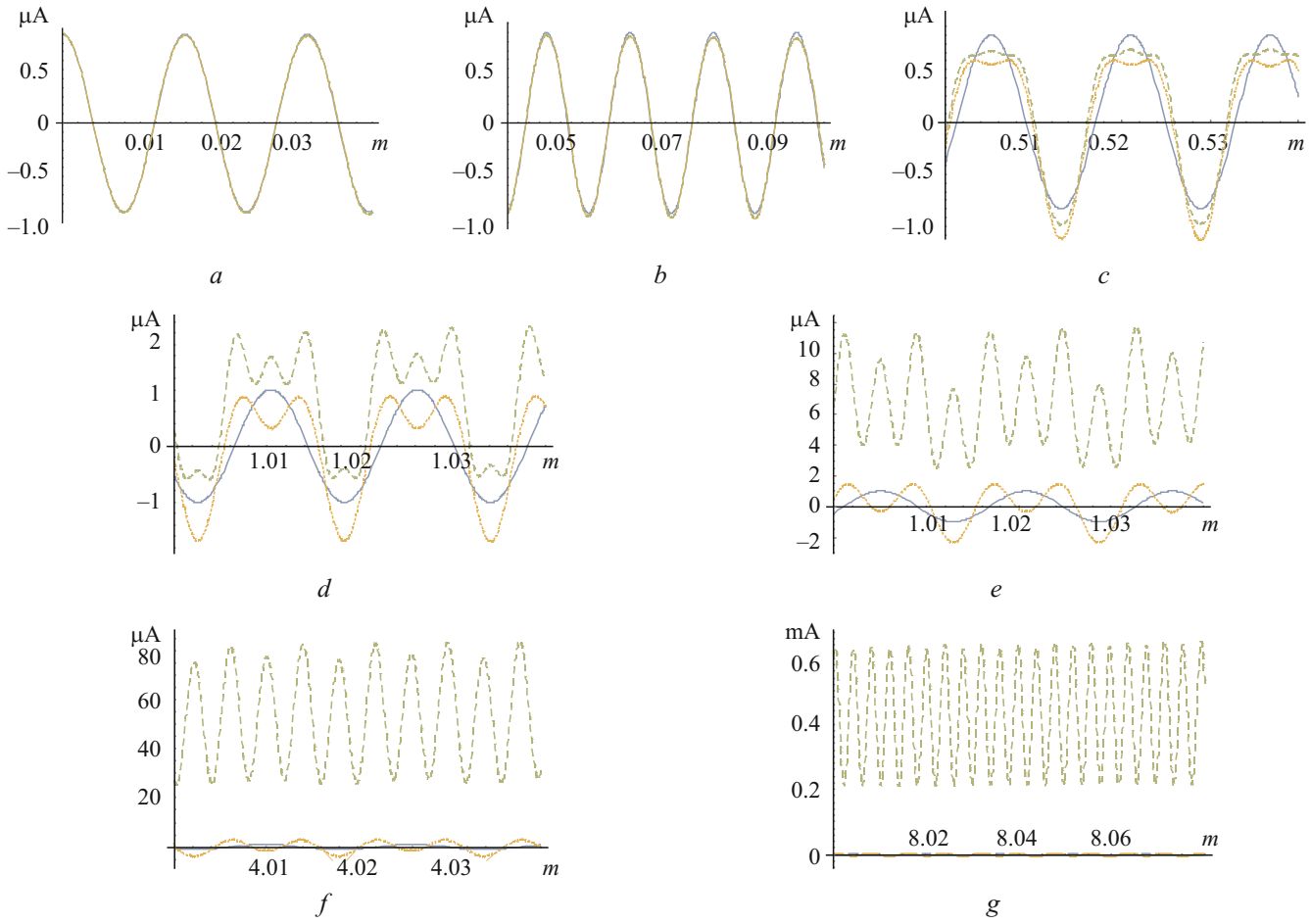

Fig. 2

Figure 2 shows the curves for M52 material, $L = 0.015$, $\omega = 1.5 \cdot 10^6$, $a_o = 1 \cdot 10^{-6}$. From the graphs, it follows that the evolution of the initial wave profile occurs for sufficiently short distances similar to the one shown in Fig. 1. Additional graphs are shown for a twofold increase in the distance of wave propagation (Fig. 2*e*), a fourfold increase in the distance (Fig. 2*f*), and an eightfold increase (Fig. 2*g*). The manifestation of nonlinearity is already more significant and the distortion of the profile is visually observable.

The evolution of the initial wave profile shows a tendency to transform into the second harmonic profile in the presence of the second approximation (halving of the wavelength and some decrease in the initial maximum amplitude) and into the fourth harmonic profile for the first three approximations (quartering of the wavelength and slight increase in the initial maximum amplitude).

It follows from the graphs that nonlinearity in both cases is manifested at different rates due to the difference in the initial parameters of the problem. Noteworthy are the solutions in the form of the first two and first three approximations typical for a harmonic wave. Both cases are represented by graphs that are asymmetric about the horizontal axis and show different rates of evolution for positive and negative amplitudes (starting from Fig. 2*c*; the velocity is higher for positive values). The graphs go down in the case of the first two approximations and go up in the case of three approximations. This shift of the graphs corresponds to the phenomenon of lowering or raising the mean value of the amplitude about which the oscillations occur. Figures 2*d–g* are intended to demonstrate this phenomenon. In a certain approximation, Fig. 2*g* shows a linear increase in the mean value of the amplitude. However, for the manifestation of this phenomenon, the distances traveled by the wave must be large.

5. Numerical Analysis of the Gaussian Wave. The initial wave profile $F(x_1) = e^{-[(a x_1)^2/2]}$ is bell-shaped and formula (18) takes the form

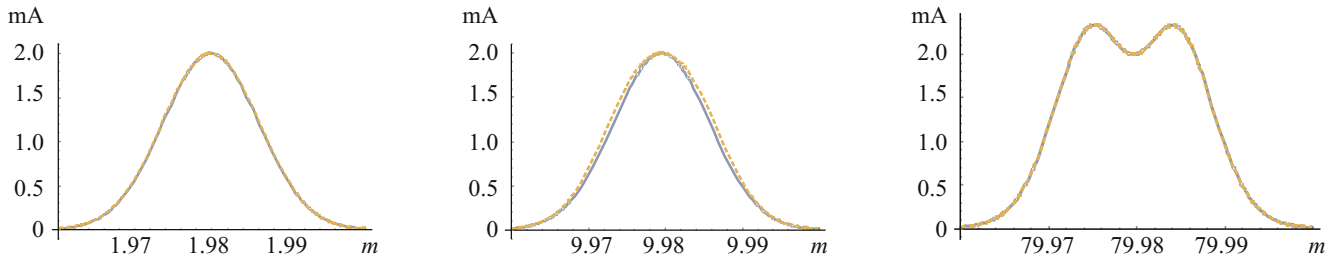

a *b* *c*

Fig. 3

$$u(x_1,t) = A^o e^{-\sigma^2/2} - (1/2)\alpha v_L a^2 t (A^o)^2 \sigma^2 e^{-\sigma^2} - (1/8)\alpha^2 v_L a^3 t (A^o)^3 \sigma^3 e^{-3\sigma^2/2}. \quad (19)$$

The concepts of first, second, and third harmonics are inapplicable, and the functions $e^{-[a^2(x_1-c_L t)^2/2]}$ and $e^{-a^2(x_1-c_L t)^2}$, $e^{-3[a^2(x_1-c_L t)^2/2]}$ can be considered the first, second, and third harmonics very approximately. However, the approximate solution (19) is very similar to solution (10). The obvious difference between solutions (10) and (19) is in that the nonlinear wave terms (21) do not explicitly depend on the wave phase $\sigma = k_L x_1 - \omega t$, whereas, for wave (19), the square in the second term and cube in the third term of wave phase $\sigma = a(x_1 - c_L t)$ appears explicitly in the expression for the amplitude.

Formula (27) was used to plot two-dimensional curves of displacement u_1 versus traveled distance x_1. There are eight sets of plots (two materials, two wavelengths, two maximum initial amplitudes). Each set includes 3 graphs for M51 material and 4 graphs for M52 material with two profiles. Figures 3*a*, 4*a*, 3*b*, and 4*b* show two superimposed profiles, one representing the first harmonic, and the other the first and second harmonics. It can be seen that nonlinearity is already observed at a distance of 50 wavelengths. Figures 3*c*, 4*c*, and 4*d* show two profiles, one corresponding to the first + second harmonics and the second to the first + second + third harmonics. Figure 4*d* is similar to Fig. 4*c*, however, corresponds to a larger distance traveled by the wave. A more developed tendency of the formation of two humps is observed here. Figures 3 and 4 differ in the initial amplitudes. For the latter, the initial amplitude and traveled distance are chosen so that nonlinearity manifests itself significantly and the distortion of the initial profile is well visually observed. In the graphs for the M51 material, the evolution of the profile is visible at a distance of about 1000 wavelengths, while for the M52 material, distances are considered an order of magnitude larger. Figure 3 shows the curves for M51 material, $L = 0.0375$, $a_o = 2.0 \cdot 10^{-3}$.

Figure 4 shows the curves for M52 material, $L = 0.0375$, $a_o = 5.0 \cdot 10^{-3}$.

From the graphs, it follows that the evolution of the initially symmetric wave profile occurs asymmetrically about the peaks—of the four slopes of the two humps, the outer (first and fourth) humps are shallower. The maximum value of the amplitude slowly increases as one hump transforms into two (see Figs. 3*a*, 4*a* and 3*b*, 4*b*). Figures 3*c*, 4*c*, and 4*d* show the graphs for the first + second and first + second + third approximations. It can be seen that the third approximation increases the peak of the first hump and decreases the peak of the second (the left peak rises and the right one falls). The central part of the graph goes down to the axis and does not cross it, separating and splicing two humps. This new phenomenon, perhaps, has not been previously described.

Thus, by allowing for the nonlinearity in analyzing the propagation of a Gaussian solitary wave, we can describe the evolution of this profile, accompanied by new wave effects.

General Conclusions. A nonlinear elastic longitudinal plane displacement wave $u(x_1, t)$ has been analyzed numerically for two types of symmetric initial profile: harmonic and bell-shaped. The wave profiles are described by two functions: trigonometrical $\cos x_1$ (e^{ix_1}) and Gaussian $e^{-x_1^2/2}$.

What all the wave profiles have in common is that they distort during propagation due to the nonlinear interaction of the wave with itself. However, these wave profiles distort differently.

A harmonic wave distorts the initial profile symmetrically relative to the upper vertex and for several sets of initial parameters at short distances (or small times) of propagation only shows a tendency to the formation of two humps for the first two approximations (formation of the second harmonic) and four humps instead of one for the first three approximations (formation of the fourth harmonic). The third approximation reveals new wave effects: the dominance of the fourth harmonic and the shift of oscillations to the first quadrant, when oscillations occur about the upwardly shifted mean value of the amplitude.

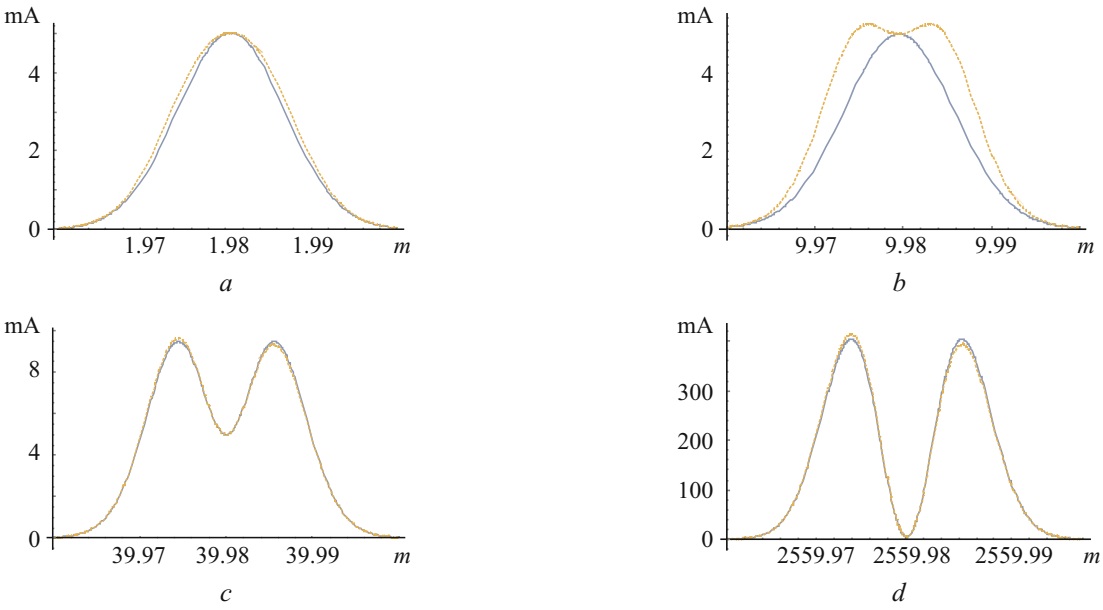

Fig. 4

A bell-shaped solitary wave no longer retains symmetry when it moves in a nonlinearly elastic medium. Like a harmonic wave, for some initial sets of parameters, this wave does not change the wavelength and only shows a tendency towards the formation of two humps instead of one when taking into account the first three approximations. At longer traveled distances, two bell-shaped waves form and adjoin each other and halve wavelength. The third approximation makes it possible to reveal new wave effects: asymmetry of the right and left humps about the peak of the hump and the asymmetry of the humps themselves about each other, the sinking of the left and elevation of the right hump.

REFERENCES

1. J. J. Rushchitsky and S. I. Tsurpal, *Waves in Microstructural Materials* [in Ukrainian], Inst. Mekh. S. P. Timoshenka, Kyiv (1998).
2. J. J. Rushchitsky, "Approximate analysis of the evolution of a longitudinal wave propagating in an elastic medium," *Dop. NAN Ukrainy*, No. 8, 46–58 (2019).
3. C. Cattani and J. Rushchitsky, *Wavelet and Wave Analysis as Applied to Materials with Micro and Nanostructure*, World Scientific, Singapore–London (2007).
4. I. S. Gradstein and I. M. Ryzhik, *Table of Integrals, Series, and Products*, 7th ed., Academic Press Inc., New York (2007).
5. A. N. Guz and J. J. Rushchitsky, "For the 100th anniversary of the S. P. Timoshenko Institute of Mechanics of the NASU: Books (monographs and textbooks) published by the institute," Int. *Appl. Mech.*, **54**, No. 2, 121–142 (2018).
6. J. J. Rushchitsky, *Elements of the Theory of Mixtures* [in Russian], Naukova Dumka, Kyiv (1991).
7. J. J. Rushchitsky, "Certain class of nonlinear hyperelastic waves: classical and novel models, wave equations, wave effects," *Int. J. Appl. Math. Mech.*, **9**, No. 12, 600–643 (2013).
8. J. J. Rushchitsky, *Nonlinear Elastic Waves in Materials*, Springer, Heidelberg (2014).
9. J. J. Rushchitsky, "On constraints for displacement gradients in elastic materials," *Int. Appl. Mech.*, **52**, No. 2, 119–132 (2016).
10. J. J. Rushchitsky, "Plane nonlinear elastic waves: approximate approaches to the analysis of evolution-plenary lecture," in: *Abstracts of 19th Int. Conf. on Dynamical System Modeling and Stability Investigations – DSMSI 2019*, Ukraine, Taras Shevchenko Kyiv National University, May 22–24 (2019), pp. 221–223.
11. J. J. Rushchitsky, "Plane nonlinear elastic waves: Approximate approaches to analysis of evolution," Ch. 3 of the book W. A. Cooper (ed.), *Understanding Plane Waves*, Nova Science Publishers, London (2019), pp. 201–220.

12. J. J. Rushchitsky, C. Cattani, and S. V. Sinchilo, “Physical constants for one type of nonlinearly elastic fibrous micro and nanocomposites with hard and soft nonlinearities,” *Int. Appl. Mech.*, **41**, No. 12, 1368–1377 (2005).
13. J. J. Rushchitsky and V. N. Yurchuk, “An approximate method for analysis of solitary waves in nonlinear elastic materials,” *Int. App. Mech.*, **52**, No. 3, 282–290 (2016).
14. V. N. Yurchuk and J. J. Rushchitsky, “Numerical analysis of the evolution of the plane longitudinal nonlinear elastic waves with different initial profiles,” *Int. App. Mech.*, **53**, No. 1, 104–110 (2017).
15. J. J. Rushchitsky and V. M. Yurchuk, “Evolution of SV-wave with Gaussian profile,” *Int. Appl. Mech.*, **53**, No. 3, 300–304 (2017).